Catalysis Science & Technology

Accepted Manuscript

ROYAL SOCIETY OF CHEMISTRY

www.rsc.org/catalysis

Catal. Sci. Technol. Catalysis Science & Technology Dynamic Article Links ►

Cite this: DOI: 10.1039/c0xx00000x

www.rsc.org/xxxxxx

Full Paper

Catalytic Reduction Mechanism of NO by CO on Rh_4^+ Cluster: A Density Functional Theory Study

Ben-Fang Su,[a] Hong-Quan Fu,[a] Hua-Qing Yang*[a] and Chang-Wei Hu[b]

Received (in XXX, XXX) Xth XXXXXXXXX 20XX, Accepted Xth XXXXXXXXX 20XX
DOI: 10.1039/b000000x

The catalytic reduction of NO by CO on Rh_4^+ cluster has been extensively studied on the ground and first excited states at B3LYP/6-311+G(2d), SDD level. The main reaction pathway includes the following elementary steps, (1) the coadsorption of NO and CO, (2) the recombination of NO and CO molecules to form CO_2 molecule and N atom, or the decomposition of NO to N and O atoms, (3) the reaction of N atom with the second adsorbed NO to form N_2O, (4) the decomposition of N_2O to N_2 molecule and O atom, and (5) the recombination of O atom and CO to form CO_2. At low temperature (300-760 K), the turnover frequency (TOF) determining transition state (TDTS) is the simultaneous C-O bond formation and N-O bond cleavage, with the rate constant (s^{-1}) of $k_{Ps} = 4.913 \times 10^{12}\exp(-272{,}724/RT)$. The formation of CO_2 should originate in half from the reaction between the adsorbed CO and NO. The presence of CO in some degree decreases the catalytic reduction temperature of NO on Rh_4^+ cluster. At high temperature (760-900 K), the TDTS is concerned to the N-O bond cleavage, with the rate constant (s^{-1}) of $k_{Pa} = 6.721 \times 10^{15}\exp(-318{,}376/RT)$. The formation of CO_2 should stem solely from the surface reaction between the adsorbed CO and O atom, the latter being originated from NO decomposition. The bridge $N_bRh_4^+$ is thermodynamically preferred. Once the bridge $N_bRh_4^+$ is formed, the N_2O and NCO contained species are predicted to exist, which is in good agreement with the experimental result.

1. Introduction

Recently, small clusters and nanoparticles have been of great interest from both the fundamental and technological viewpoints, since its catalytic reactivity is substantially modified by changing their size, structure, charge sate, and chemical composition.[1] Metallic rhodium has proved to be one of the best components for the removal of NO_x, a very important step in pollution-control processes.[2,3] The catalytic reduction mechanism of NO_x by CO on rhodium-based catalysts is of great practical importance in designing suitable automotive exhaust gas catalysts.[4-6] Thereupon, the catalytic mechanism of various types of Rh clusters has received a lot of attention with respect to the reduction of NO_x by CO.

Using Fourier transform ion cyclotron resonance (FT-ICR) mass spectrometry, Anderson et al. and Ford et al. have revealed the high activity of $Rh_n^{\pm}(n < 30)$ cluster toward the dissociation of the NO molecule,[7,8] in which the cationic clusters react significantly faster than the anions. By means of density functional theory calculations, Ghosh et al. have studied the binding of NO to the small rhodium clusters including one to five atoms,[9] indicating that the rhodium clusters may be good catalysts for NO reduction. Torres et al. have confirmed the dissociative adsorption of NO on Rh_6^+.[10] Xie et al. have analyzed the NO adsorption and decomposition reaction mechanism on Rh_7^+ cluster, which includes NO adsorption, NO decomposition to N and O atoms, and the N atom reaction with the second adsorbed NO and then reduction to N_2 molecule.[11] Romo-Ávila et al. have investigated the stability and dissociation behavior of NO molecules adsorbed on small nonmagnetic $Rh_n^{0,\pm}$ cluster (n = 3, 4, 6, and 13).[1] They proposed that the dissociation of the N-O bond is more easily obtained on square facets than on triangular atomic environments, and that the energy barriers to break the N-O bond depend on the charge state of the systems.[1] Zeinalipour-Yazdi et al. have performed a systematic study on the adsorption of CO on a Rh_4 cluster,[12] indicating the vertical adsorption of CO to the metal-metal bond. Later, Xie et al. have explored the catalytic reduction mechanism of NO by CO on Rh_7^+ cluster.[13] They suggested that the reaction proceeds via the following steps, the coadsorption of NO and CO on the Rh_7^+ cluster, then the decomposition of adsorbed NO into N and O atoms, the reaction of O atom with the adsorbed CO to form CO_2 molecule, the adsorption of the second NO on the Rh_7^+ cluster, the decomposition of the adsorbed NO into N and O atoms, the coupling of two N atoms to yield N_2 molecule, and the recombination of the second CO of O atom to CO_2 molecule, in

which the second adsorbed NO generating N and O atoms is the rate-limiting step of whole catalytic cycle.[13] These theoretical study supports that the NO molecule dissociates into N and O atoms, and the mechanism of CO_2 formation accords to the recombination of CO and O atom, the latter originating from the NO decomposition.[1,11-13]

Nevertheless, the mechanism of CO_2 formation is experimentally in debate, one through the reaction between CO and NO,[14] and another through recombination of CO and O atom, the latter originating from the NO decomposition.[15-17] Lately, we have investigated the reaction mechanism of NO and CO catalyzed by Rh atom,[18] which involves two main reaction stages, NO deoxygenation to generate N_2O and then the deoxygeneation of N_2O with CO to form N_2 and CO_2. The key reaction step is the NO deoxygenation to generate N_2O, in which the self-deoxygenation of NO reaction pathway is kinetically more preferable than that in the presence of CO.[18] Moreover, on the single Rh atom, CO plays a dominating role in the RhO reduction to regenerate Rh atom.[18]

To probe the cooperativity of Rh-Rh toward the NO reduction by CO, the Rh_4^+ cluster are preferred in the present study, since the cationic clusters react significantly faster than the anions.[7,8] During the NO and CO conversion process, the intermediate N_2O, NCO, and CN groups were experimentally observed.[19,20] In the catalytic conversion of $2NO + 2CO \rightarrow N_2 + 2CO_2$, there are also a number of concomitant channels yielding N_2O, NCO, and CN, which complicates a comprehensive understanding.[4,21,22] Therefore, of particular interest is to explore the complete catalytic reduction mechanism of NO by CO on the Rh_4^+ cluster in conjunction with the relevant side reactions, as exemplified by the reactions

$2NO + 2CO \rightarrow N_2 + 2CO_2$ (1)

$NO + 2CO \rightarrow NCO + CO_2$ (2)

$NO + 3CO \rightarrow CN + 2CO_2$ (3)

The aims of the present study are as follows: (a) to elucidate the determining transition state (TDTS) and the determining intermediate (TDI) of the turnover frequency (TOF), (b) to obtain a better understanding of the preference of reaction pathway, and (c) to gain an deep insight into the cooperativity of Rh-Rh on catalytic reduction mechanism.

2. Computational details

All calculations were carried out with the Gaussian 09 program package.[23] Full geometry optimizations were run to locate all the stationary points and transition states (TSs) on the ground and first excited states. The B3LYP[24,25] functional method was employed with the 6-311+G(2d) basis set for carbon, nitrogen, and oxygen,[26,27] and the Stuttgart/Dresden (SDD) basis set and the corresponding effective core potential (ECP) for rhodium,[28] namely B3LYP/6-311+G(2d), SDD. Moreover, the stability of the wavefunction of the auxiliary Kohn-Sham determinant in density function theory (DFT) was tested.[29,30] If an instability is found, the wavefunction is reoptimized with appropriate reduction in constraints, and the stability tests and reoptimizations are repeated until a stable wavefunction is found.[29,30] Computed $<S^2>$ values suggested that only small spin contamination is included in the calculations. Systematic frequency calculations were performed to characterize stationary points obtained and to take corrections of zero-point energy (ZPE) into account. For the reaction pathway analysis, every transition structure has a unique imaginary frequency, and the connections between transition states and corresponding intermediates were verified by means of intrinsic reaction coordinate (IRC) calculations.[31,32] The dominant occupancies of natural bond orbitals and dominant stabilization energies $E(2)$ between donors and acceptors for some species have been analyzed with the help of the natural bond orbital (NBO) analysis.[33,34] Unless otherwise mentioned, the Gibbs free energy of formation (ΔG) for species is relative to the initial ground state reactants including ZPE correction obtained at B3LYP/6-311+G(2d), SDD level in the gas phase under atmospheric pressure and room temperature (300 K and 1 atm). The changes of Gibbs free energy for the reaction (ΔG_r) were computed using the Eqs. (i).

$$\Delta G_r = \Delta G_{pro} - \Delta G_{rea} \quad \text{(i)}$$

where ΔG_{pro} and ΔG_{rea} are the Gibbs free energy of formation for products and reactants in the reaction, respectively.

The turnover frequency (TOF) of the catalytic cycle determines the efficiency of the catalyst. Based on the transition state theory,[35,36] TOF can be calculated by Eqs. ((ii) and (iii)),[37-39] in which δE (the energetic span[40]) is defined as the energy difference between the summit and trough of the catalytic cycle. G_{TDTS} and G_{TDI} are the Gibbs free energies of the TOF determining transition state (TDTS) and the TOF determining intermediate (TDI), and ΔG_r is the global free energy of the whole cycle.

$$\mathrm{TOF} = \frac{k_b T}{h} e^{-\frac{\delta E}{RT}} \quad \text{(ii)}$$

$$\delta E = \begin{pmatrix} G_{TDTS} - G_{TDI} & \text{if TDTS appears after TDI} \\ G_{TDTS} - G_{TDI} + \Delta G_r & \text{if TDTS appears before TDI} \end{pmatrix} \quad \text{(iii)}$$

where k_b is the Boltzmann constant, T is the absolute temperature, and h is the Plank constant.

The rate constants (k) have been evaluated according to conventional transition state theory $k(T)$ (TST), based on Winger's formulation as follows[41]:

$$k(T) = \frac{k_B T}{hc^0} e^{\frac{-\Delta G^{\neq}}{k_B T}} \quad \text{(iii)}$$

where k_B is the Boltzmann constant, T is the absolute temperature, h is the Plank constant, c^0 is the standard concentration (1 mol dm^{-3}), and $\Delta G^{\neq}$ is the activation Gibbs free energy barrier.

3. Results and Discussion

The same method and basis sets (B3LYP/6-311+G(2d), SDD) were successfully used to perform the geometric structure optimization in the reaction mechanisms of methane catalyzed by the neutral RhO,[42] the cation RhO^+,[43] and the $Rh/\gamma\text{-}Al_2O_3$ model catalyst,[44] and in the catalytic reduction mechanism of NO by CO on the Rh atom.[18] Thereupon, the present method and basis sets should be appropriate for the present system ($Rh_4^+ + NO + CO$).

As mentioned earlier, the N_2O and NCO are regarded as the

important intermediates in the NO and CO conversion

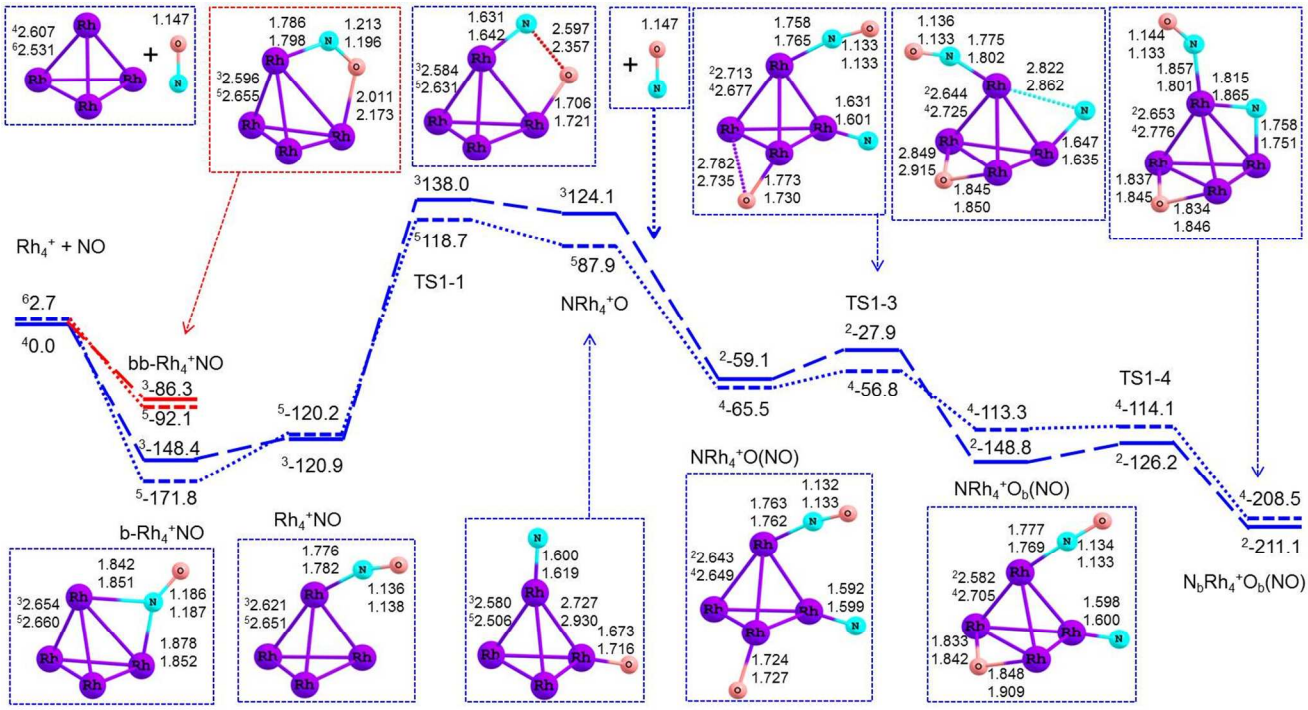

(a)

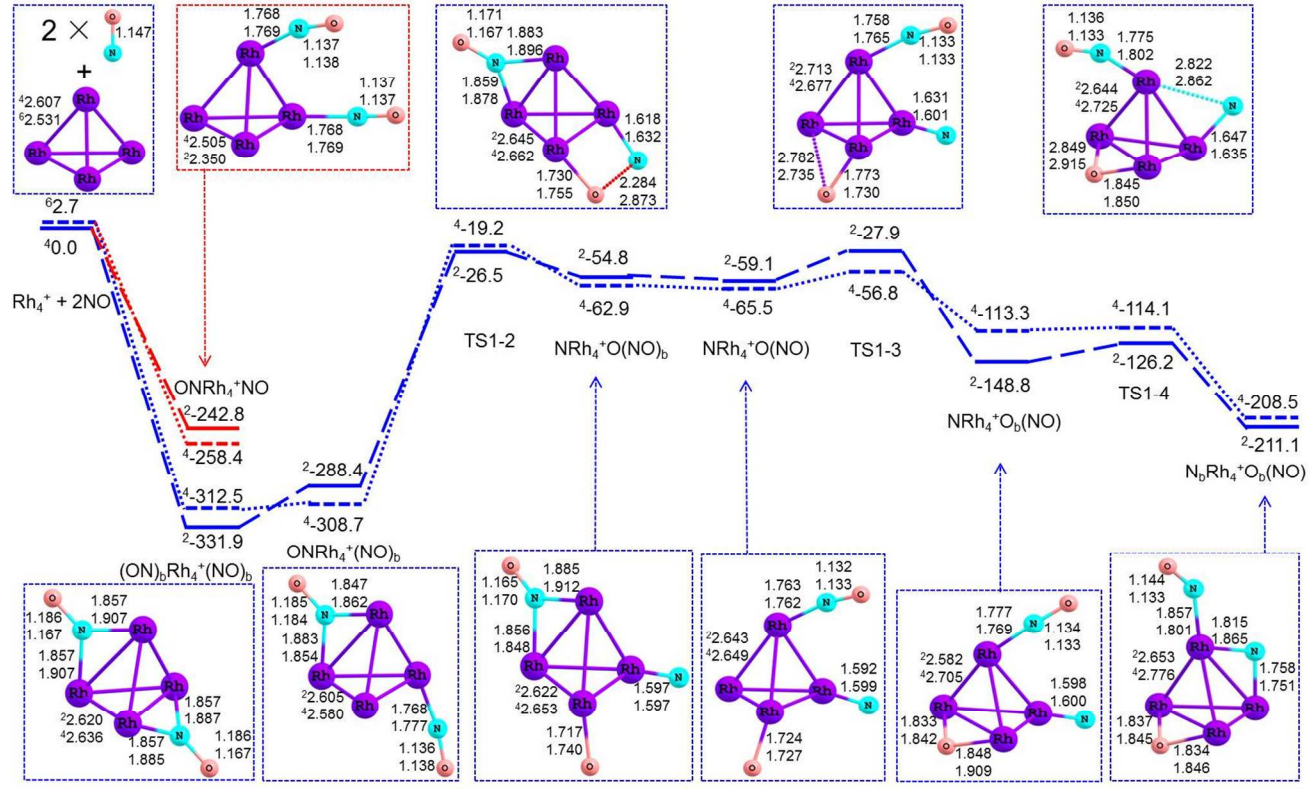

(b)

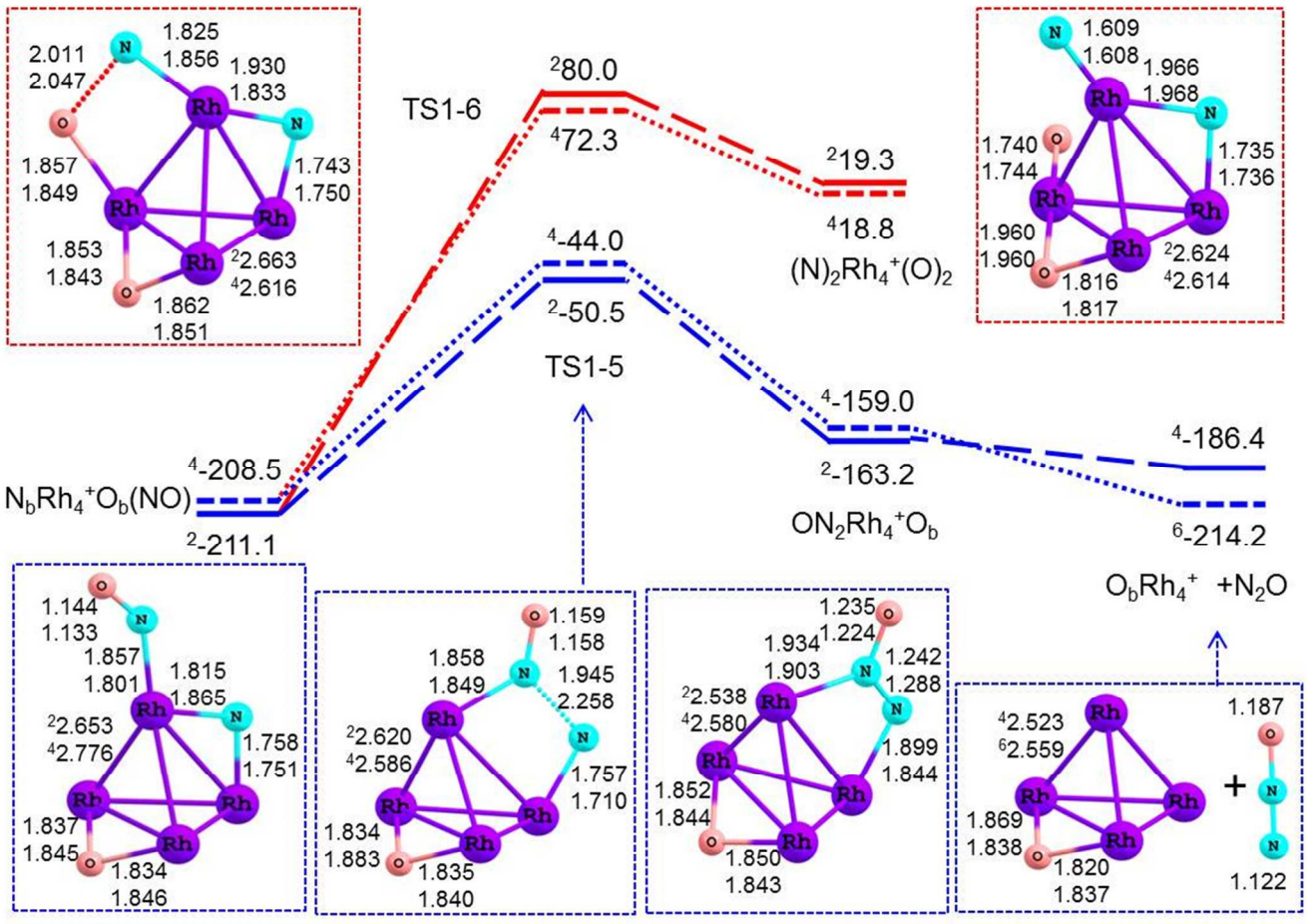

(c)

Fig.1 The geometric structures of the reactants, intermediates, TSs, and products, and the schematic energy diagrams for the reaction (4) $Rh_4^+ + 2NO \rightarrow O_bRh_4^+ + N_2O$ calculated at the B3LYP/6-311+G(2d), SDD level. Bond lengths are reported in Å and bonds angles in degree. Relative energies (kJ mol^{-1}) for the corresponding species relative to $^4Rh_4^+ + 2NO$ are shown. (a), for the $Rh_4^+ + 2NO \rightarrow N_bRh_4^+O_b(NO)$ reaction stage with the N-O bond cleavage in the absence of the second NO molecule; (b), for the $Rh_4^+ + 2NO \rightarrow N_bRh_4^+O_b(NO)$ reaction stage with the N-O bond cleavage in the presence of the second NO molecule; (c), for the $N_bRh_4^+O_b(NO) \rightarrow O_bRh_4^+ + N_2O$ reaction stage.

processes.[19,20] Furthermore, N_2O dissociation has been observed by infrared induced reactivity on the surface of small gas-phase rhodium clusters.[45,46] In this study, we will mainly discuss the following six reactions.

$Rh_4^+ + 2NO \rightarrow O_bRh_4^+ + N_2O$ (4)

$Rh_4^+ + N_2O \rightarrow O_bRh_4^+ + N_2$ (5)

$O_bRh_4^+ + CO \rightarrow Rh_4^+ + CO_2$ (6)

$Rh_4^+ + NO + CO \rightarrow N_bRh_4^+ + CO_2$ (7)

$N_bRh_4^+ + NO \rightarrow Rh_4^+ + N_2O$ (8)

Furthermore, the following two side reactions will also be discussed to generalize overall reduction mechanism of NO by CO on the Rh_4^+ cluster.

$N_bRh_4^+ + CO \rightarrow Rh_4^+ + NCO$ (9)

$Rh_4^+ + NCO \rightarrow O_bRh_4^+ + CN$ (10)

Accomplishing the main reaction (1) of $2NO + 2CO \rightarrow N_2 + 2CO_2$, there are two kinds of catalytic cycles. One is made up of the (4), (5), and 2×(6)reactions through N-O bond cleavage in the absence of CO, and another is composed of the (7), (8), (5), and (6) reactions through N-O bond cleavage in the presence of CO, denoted as the reaction pathways A and P (**RP-A** and **RP-P**), respectively. It is obvious that the main difference in the two catalytic cycles originates from the reaction pathways for the N_2O formation. Achieving the side reaction (2) of $NO + 2CO \rightarrow NCO + CO_2$, there is a unique reaction pathway, which is composed of the (7) and (9) reactions through N-O bond cleavage in the presence of CO. Acquiring the side reaction (3) of $NO + 3CO \rightarrow CN + 2CO_2$, there is a unique reaction pathway, which comprises the (7), (9), (10), and (6) reactions through N-O bond cleavage in the presence of CO. The ΔG_r values of the (1), (2), and (3) reactions are calculated to be -696.4, -114.1, and -74.5 kJ mol^{-1}, respectively. Thereupon, all the three reactions are thermodynamically preferable. Then, we will discuss the kinetics of the above three reactions (1), (2), and (3), and the competition of the catalytic cycles, as well as the selectivity of main and side reactions infra.

Moreover, particular attention was devoted to the possible occurrence of a two-state reactivity phenomenon, since the spin crossing is often involved in the transition-metal-containing reactions.[47] Therefore, the potential energy profiles for the ground and the first excited states of rhodium-containing reactions were investigated. The superscript prefixes "2", "3", "4", "5", "6", and "7" will be used to indicate the doublet, triplet, quartet, quintet, sextet, and septet states, respectively.

Cite this: DOI: 10.1039/c0xx00000x

www.rsc.org/xxxxxx

Full Paper

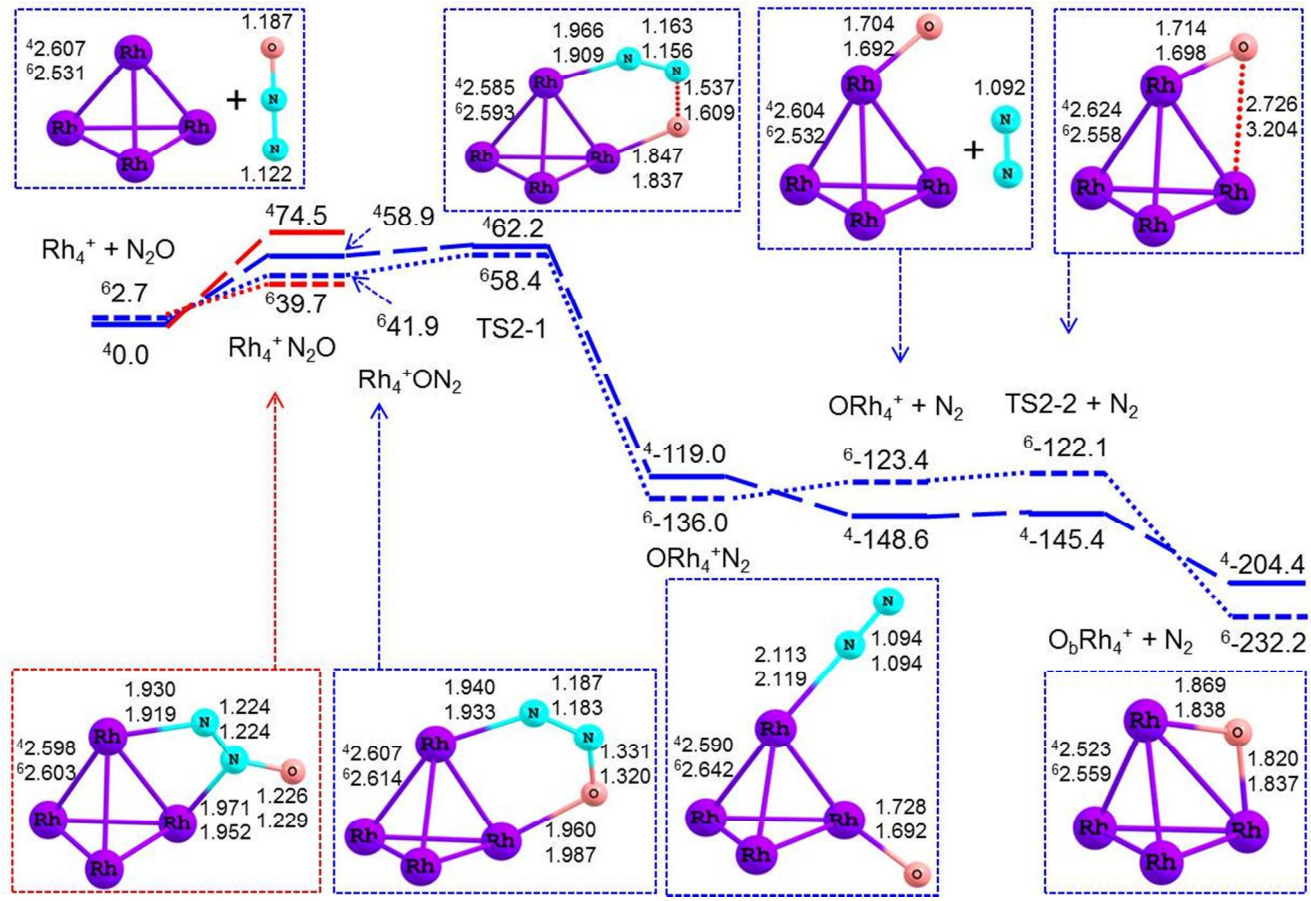

Fig. 2 The geometric structures of the reactants, intermediates, TSs, and products, and the schematic energy diagrams for the reaction (5) $Rh_4^+ + N_2O \rightarrow O_bRh_4^+ + N_2$ calculated at the B3LYP/6-311+G(2d), SDD level. Bond lengths are reported in Å and bonds angles in degree. Relative energies (kJ mol^{-1}) for the corresponding species relative to $^4Rh_4^+ + N_2O$ are shown.

3.1 The RP-A for 2NO + 2CO → N_2 + 2CO_2

This reaction pathway **RP-A** can proceed via four steps, NO adsorption, NO decomposition to N and O atoms, the reaction of N atom with another adsorbed NO and then reduction to N_2 molecule and O atom, and the recombination of CO and O atom to form CO_2. The **RP-A** can be further divided into two reaction pathways, through N-O bond cleavage in the absence and presence of another NO molecule, denoted as "**RP-Aa**" and "**RP-Ap**", respectively. The **RP-A** falls into three sequent reactions of (4), (5), and 2×(6). Next, it is necessary to investigate the above three reactions, both thermodynamically and kinetically.

3.1.1 $Rh_4^+ + 2NO \rightarrow O_bRh_4^+ + N_2O$

The geometric structures and the schematic energy diagrams for the reaction of (4) $Rh_4 + 2NO \rightarrow O_bRh_4^+ + N_2O$ are depicted in Figs. 1a-1c, respectively. As indicated in Fig. 1a, the quartet state Rh_4^+ cluster is the ground state, with the Mulliken atomic spin densities of 1.30, 1.51, 1.65, and -1.46 *e* and the natural charge of 0.15, 0.22, 0.30, and 0.32 for the four Rh atoms, respectively. The sextet state Rh_4^+ clusters lies 2.7 kJ mol^{-1} above the ground quartet state, with the Mulliken atomic spin densities of 0.03, 1.57, 1.70, and 1.71 *e* and the natural charge of 0.19, 0.24, 0.29, and 0.29 for the four Rh atoms, respectively. The doublet state Rh_4^+ clusters locates 31.1 kJ mol^{-1} above the ground quartet state, with the Mulliken atomic spin densities of 1.15, 1.15, -0.65, and -0.66 *e* for the four Rh atoms, respectively, and the natural charge of 0.25 for each Rh atom. Thereupon, we will discuss the relevant reactions on the ground quartet state $^4Rh_4^+$ and the first excited state $^6Rh_4^+$. The reaction of (4) is calculated to be exergonic by 214.2 kJ mol^{-1} on its minimal energy reaction pathway (MERP). It is shown that this reaction is thermodynamically preferable. Then, we will infra discuss its kinetics from potential energy surfaces (PESs).

As shown in Fig. 1a for **RP-Aa**, when one NO molecule is initially adsorbed on Rh_4^+ cluster, there are three kinds of configurations through N-end, one top Rh_4^+NO, one bridge b-Rh_4^+NO, and one bridge-bridge bb-Rh_4^+NO with the stabilization energies of 120.9, 171.8, and 92.1 kJ mol^{-1} on the respective ground state, respectively. Among these three configurations, the

Cite this: DOI: 10.1039/c0xx00000x

www.rsc.org/xxxxxx

Full Paper

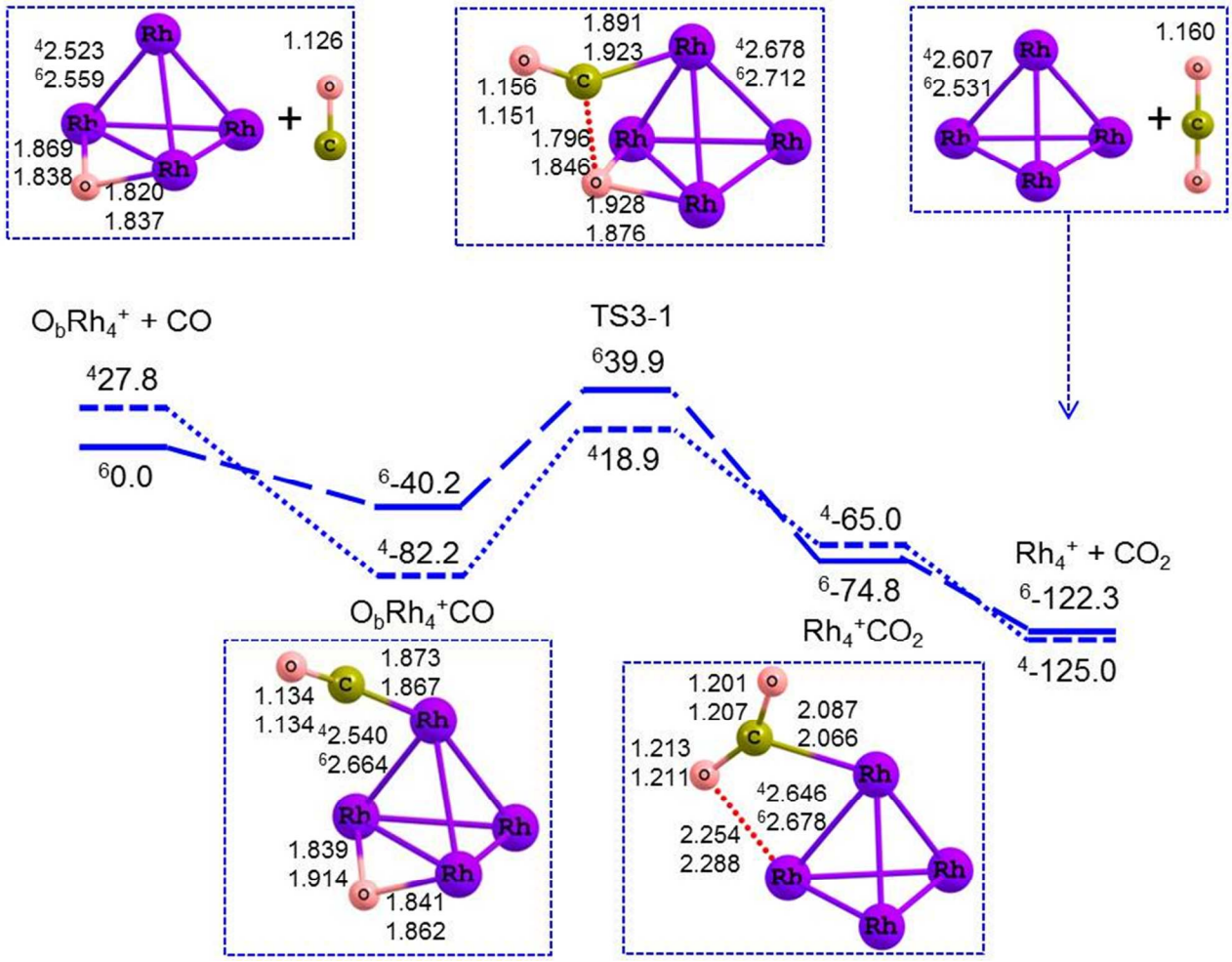

Fig. 3 The geometric structures of the reactants, intermediates, TSs, and products, and the schematic energy diagrams for the reaction (6) $O_bRh_4^+ + CO \rightarrow Rh_4^+ + CO_2$ calculated at the B3LYP/6-311+G(2d), SDD level. Bond lengths are reported in Å and bonds angles in degree. Relative energies (kJ mol^{-1}) for the corresponding species relative to $^6O_bRh_4^+ + CO$ are shown.

bridge ^{5}b-Rh_4^+NO is the most thermodynamically preferable. In ^{5}b-Rh_4^+NO, the spin densities of –Rh_4 and –NO moieties are 4.17 and -0.17 *e*. It is indicated that the unpaired electrons are mainly on –Rh_4 moiety. Moreover, the occupancies of each Rh-N bond orbital are 1.94 *e*, indicating a complete single-bond in Rh-N. The bridge b-Rh_4^+NO can isomerize into the top Rh_4^+NO with the energy barrier of 50.9 kJ mol^{-1} on its MERP. Next, the N-O bond scission takes place to form a top-top configuration NRh_4^+O via a four-member TS1-1. Then, when another NO molecule is adsorbed on Rh_4^+ cluster, a molecular complex $NRh_4^+O(NO)$ is engendered. From $NRh_4^+O(NO)$, the [1,2]-O and [1,2]-N shifts sequently take place via TS1-3 and TS1-4, respectively, to produce a more stable bridge-bridge $N_bRh_4^+O_b(NO)$. As shown in Fig. 1a, the triplet-quintet spin crossing should take place near TS1-1 via the minimum energy crossing point (MECP) between $^3Rh_4^+$NO and $^5Rh_4^+$NO. Moreover, the doublet-quartet spin crossing should occur near TS1-3 via the MECP between $^4NRh_4^+O_b(NO)$ and $^2NRh_4^+O_b(NO)$. Thereupon, the MERP should start at the quartet state and end on the doublet one, with an exergonic value of 211.1 kJ mol^{-1}.

As depicted in Fig. 1b for **RP-Ap**, when two NO molecules are initially adsorbed on Rh_4^+ cluster simultaneously, there are three kinds of configurations through N-end, one top-top $ONRh_4^+NO$, one top-bridge $ONRh_4^+(NO)_b$, and one bridge-bridge $(ON)_bRh_4^+(NO)_b$ with the stabilization energies of 258.4, 308.7, and 331.9 kJ mol^{-1} on the respective ground state, respectively. Among these three configurations, the bridge-bridge $(ON)_bRh_4^+(NO)_b$ is the most thermodynamically favorable. In $^2(ON)_bRh_4^+(NO)_b$, the spin densities of –Rh_4 and –NO moieties are 1.50 and -0.50 *e*. It is indicated that the unpaired electrons exist both on –Rh_4 and –NO moieties. Moreover, the occupancies of each Rh-N bond orbitals are 1.61 *e*, indicating an approximate

single-bond in each Rh-N. The bridge-bridge $(ON)_bRh_4^+(NO)_b$ can isomerize into the top-bridge $ONRh_4^+(NO)_b$ with the energy barrier of 23.2 kJ mol^{-1}. Next, one N-O bond cleavage occurs to form a molecular complex $NRh_4^+O(NO)_b$ via a four-member TS1-2. $NRh_4^+O(NO)_b$ readily converts into the isomer $NRh_4^+O(NO)$ without any energy requirement. As mentioned earlier, from $NRh_4^+O(NO)$, the [1,2]-O and [1,2]-N shifts sequently occur via TS1-3 and TS1-4, respectively, to produce a more stable bridge-bridge $N_bRh_4^+O_b(NO)$. As shown in Fig. 1b, the doublet-quartet spin crossing should take place twice near TS1-2 and TS1-3 via two MECPs between $^4ONRh_4^+(NO)_b$ and $^2ONRh_4^+(NO)_b$, and between $^4NRh_4^+O_b(NO)$ and $^2NRh_4^+O_b(NO)$. Then, the MERP should start at the quartet state and end on the doublet state.

As shown in Fig. 1c, there are two reaction pathways from $N_bRh_4^+O_b(NO)$ to $(N)_2Rh_4^+(O)_2$ and $O_bRh_4^+ + N_2O$, respectively. One is the N-N bond formation via a four-member TS1-5, to yield a molecular complex $ON_2Rh_4^+O_b$. Another is the N-O bond cleavage via a four-member TS1-6, to form $(N)_2Rh_4^+(O)_2$. It is obvious that the two reaction pathways are competitive. Because the doublet ^{2}TS1-5 locates 122.8 kJ mol^{-1} below the quartet ^{4}TS1-6 on their MERPs, the reaction pathway of the N-N bond formation is more kinetically favorable than that of the N-O bond cleavage. Thereupon, the reaction pathway of N-O bond cleavage should be ruled out. Last, $ON_2Rh_4^+O_b$ set the N_2O molecule free without any energy requirement, leaving $O_bRh_4^+$ behind.

On account of Figs. 1a-1c, for **RP-Aa**, the MERP should include the highest energy barrier (HEB) of 239.6 kJ mol^{-1} at the N-O bond cleavage step of $^3Rh_4^+NO \rightarrow {}^5$TS1-1, with the energy height of the highest point (EHHP) of 118.7 kJ mol^{-1} at ^{5}TS1-1. On the other hand, for the **RP-Ap**, the MERP should involve the HEB of 282.2 kJ mol^{-1} at the N-O bond cleavage step of $^4ONRh_4^+(NO)_b \rightarrow {}^2$TS1-2 and the EHHP of 0.0 kJ mol^{-1} at the entrance. For the reaction of $Rh_4^+ + 2NO \rightarrow O_bRh_4^+ + N_2O$, the MERP should starts at the quartet state and end on the sextet one.

3.1.2 $Rh_4^+ + N_2O \rightarrow O_bRh_4^+ + N_2$

The geometric structures and the schematic energy diagrams for the reaction of (5) $Rh_4^+ + N_2O \rightarrow O_bRh_4^+ + N_2$ are depicted in Fig. 2. As shown in Fig. 2, the reaction of (5) is calculated to be exergonic by 232.2 kJ mol^{-1} on its MERP. Therefore, this reaction is thermodynamically preferable. Initially, when one N_2O molecule interacts with Rh_4^+ cluster, two kinds of configurations are obtained, μ-1,3-O,N $Rh_4^+ON_2$ and μ-1,2-N,N $Rh_4^+N_2O$ with the energy requirement of 41.9 and 39.7 kJ mol^{-1} on their MERPs, respectively. It is indicated that both $Rh_4^+ON_2$ and $Rh_4^+N_2O$ are not thermodynamically stable, which may stem from the decrease of entropy, because of the relative electronic energies of -4.1 and -5.6 kJ mol^{-1} relative to the discrete Rh_4^+ and N_2O, respectively, on their MERPs. Second, from $Rh_4^+ON_2$, the N-O bond cleavage and the Rh-O bond formation take place simultaneously via a five-member TS2-1, to yield a molecular complex $ORh_4^+N_2$. Third, $ORh_4^+N_2$ releases the free N_2 molecule, keeping ORh_4^+ behind. Finally, from the top ORh_4^+, the [1,2]-O migration occurs via a three member TS2-2, to produce a more stable bridge $O_bRh_4^+$.

As depicted in Fig. 2, for the reaction of $Rh_4^+ + N_2O \rightarrow O_bRh_4^+ + N_2$, the quartet-sextet spin crossing should take place thrice near TS2-1 and TS2-2. Therefore, the MERP should start at the quartet state and terminate on the sextet one, with the HEB of 41.9 kJ mol^{-1} at $^4Rh_4^+ + N_2O \rightarrow {}^6Rh_4^+ON_2$ reaction step and the EHHP of 58.4 kJ mol^{-1} at ^{6}TS2-1.

3.1.3 $O_bRh_4^+ + CO \rightarrow Rh_4^+ + CO_2$

The geometric structures and the schematic energy diagrams for the reaction of (6) $O_bRh_4^+ + CO \rightarrow Rh_4^+ + CO_2$ are depicted in Fig. 3. As shown in Fig. 3, the reaction of (6) is calculated to be exergonic by 125.0 kJ mol^{-1} on its MERP. Thereby, this reaction is thermodynamically preferable. First, one CO molecule is adsorbed on $O_bRh_4^+$ through C-end, forming a molecular complex $O_bRh_4^+CO$. Second, [1,3]-O shift occurs via a four-member TS3-1, to yield a molecular complex $Rh_4^+CO_2$. Last, $Rh_4^+CO_2$ set the CO_2 molecule free without any energy requirement, leaving Rh_4^+ cluster behind, and then making the Rh_4^+ cluster reduced and completing the catalytic cycle.

As indicated in Fig. 3, the quartet-sextet spin crossing should occur near TS3-1. Then, the MERP should begin on the sextet state and end on the quartet one, with the HEB of 101.1 kJ mol^{-1} at the C-O bond formation step of $^4O_bRh_4^+CO \rightarrow {}^4$TS3-1 and the EHHP of 18.9 kJ mol^{-1} at ^{4}TS3-1.

As mentioned earlier, for the gross reaction $2NO + 2CO \rightarrow N_2 + 2CO_2$, there are two reaction pathways **RP-Aa** and **RP-Ap**. The TOF analysis showed that the TDI and TDTS for **RP-Aa** are ^{5}b-Rh_4^+NO and ^{5}TS1-1, respectively, and that the TDI and TDTS for **RP-Ap** are $^2(ON)_bRh_4^+(NO)_b$ and ^{2}TS1-2, respectively. The TDIs ^{5}b-Rh_4^+NO and $^2(ON)_bRh_4^+(NO)_b$ are concerned to the NO adsorbed molecularly on Rh_4^+ cluster. The TDTSs, ^{5}TS1-1 and ^{2}TS1-2, answer for the N-O bond cleavage. Then, the rate constants of ^{5}b-$Rh_4^+NO \longrightarrow {}^5$TS1-1 ($k_{Aa}$) and $^2(ON)_bRh_4^+(NO)_b \longrightarrow {}^2$TS1-2 ($k_{Ap}$) are representative of the gross rate constant of the **RP-Aa** and **RP-Ap** for the reaction $2NO + 2CO \rightarrow N_2 + 2CO_2$. Over the 300-900 K temperature range, the rate constants k_{Aa} and k_{Ap} can be adapted by the following expression (in s^{-1}):

$$k_{Aa} = 4.497 \times 10^{13} \exp(-295{,}596 / RT) \quad \text{(iii)}$$

$$k_{Ap} = 1.296 \times 10^{15} \exp(-350{,}086 / RT) \quad \text{(iv)}$$

Over the 300-900 K temperature range, the rate constant k_{Aa} is two to seven magnitude orders greater than the rate constant k_{Ap}. Therefore, the **RP-Aa** is kinetically more favorable than the **RP-Ap**. It is indicated that the **RP-Aa** is dominated, compared with the **RP-Ap**. In other words, the **RP-Ap** should be ruled out, compared with **RP-Aa**. It is obvious that the presence of the second NO molecule in some degree hampers the first N-O bond cleavage, which originates from the oxidizability of NO.

3.2 The RP-P for $2NO + 2CO \rightarrow N_2 + 2CO_2$

This reaction pathway **RP-P** is composed of the four sequent reactions of (7), (8), (5), and (6). Because the reactions of (5) and (6) have been discussed earlier, it is necessary to investigate the reactions of (7) and (8), both thermodynamically and kinetically. The reaction pathway **RP-P** can be divided into two reaction pathways, through the C-O bond formation after N-O cleavage and the simultaneous C-O bond formation and N-O bond cleavage, denoted as "**RP-Pa**" and "**RP-Ps**", respectively. The **RP-Pa** proceeds via six steps, (1) the coadsorption of NO and CO, (2) the decomposition of NO to N and O atoms, (3) the recombination of CO and O atom to form CO_2, (4) the reaction of N atom with the second adsorbed NO to form N_2O, (5) the

Cite this: DOI: 10.1039/c0xx00000x

www.rsc.org/xxxxxx

Full Paper

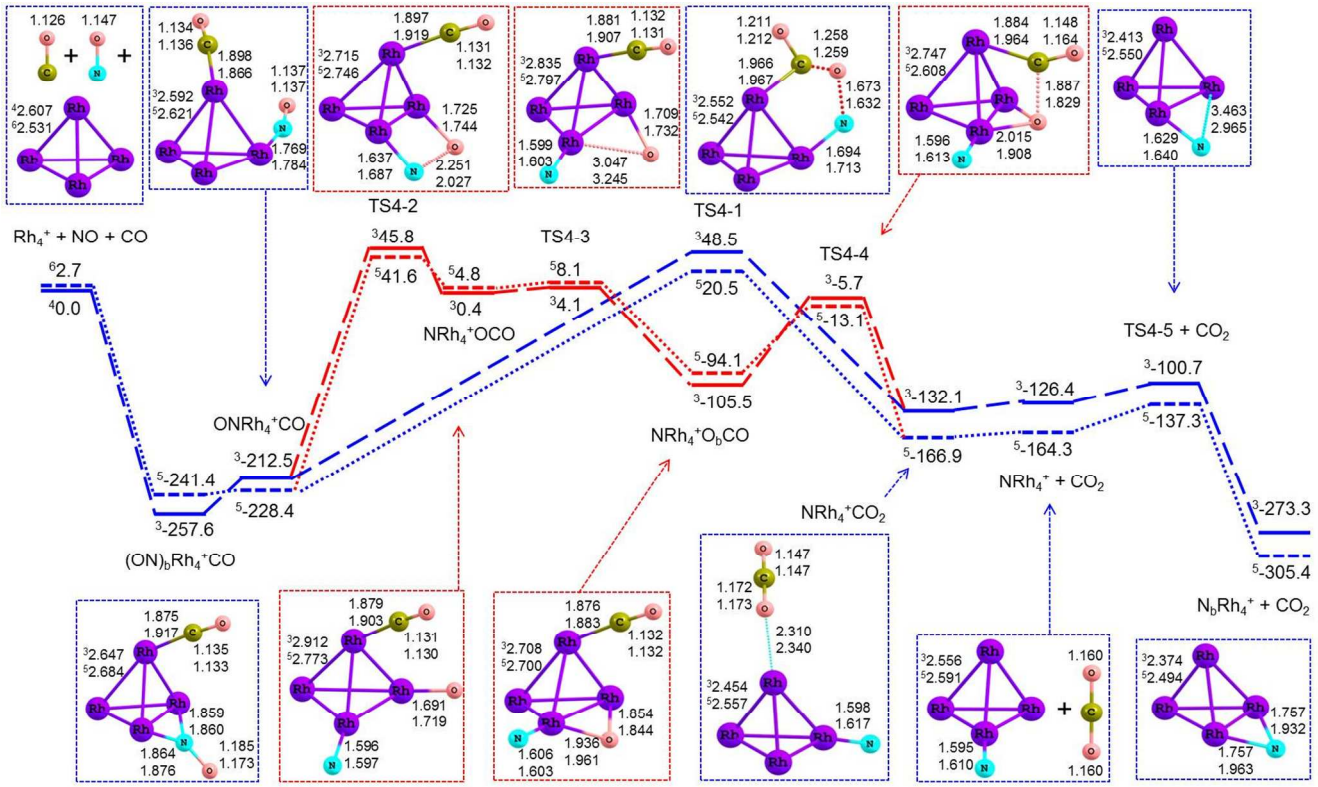

Fig. 4 The geometric structures of the reactants, intermediates, TSs, and products, and the schematic energy diagrams for the reaction (7) $Rh_4^+ + NO + CO \rightarrow N_bRh_4^+ + CO_2$ calculated at the B3LYP/6-311+G(2d), SDD level. Bond lengths are reported in Å and bonds angles in degree. Relative energies (kJ mol^{-1}) for the corresponding species relative to $^4Rh_4^+ + NO + CO$ are shown.

decomposition of N_2O to N_2 molecule and O atom, and (6) the recombination of CO and O atom to again form CO_2. The **RP-Ps** goes ahead via five steps, (1) the coadsorption of NO and CO, (2) the recombination of CO and NO molecules to form CO_2 molecule and N atom, (3) the reaction of N atom with the second adsorbed NO to form N_2O, (4) the decomposition of N_2O to N_2 molecule and O atom, and (5) the recombination of CO and O atom to again form CO_2. That is to say, the difference between **RP-Pa** and **RP-Ps** exists in the second step, N-O bond cleavage or the simultaneous C-O bond formation and N-O bond cleavage.

3.2.1 $Rh_4^+ + NO + CO \rightarrow N_bRh_4^+ + CO_2$

The geometric structures and the schematic energy diagrams for the reaction of (7) $Rh_4^+ + NO + CO \rightarrow N_bRh_4^+ + CO_2$ are depicted in Fig. 4. As shown in Fig. 4, the reaction of (7) is calculated to be exergonic by 305.4 kJ mol^{-1} on its MERP. Thereupon, this reaction is thermodynamically preferable. At the beginning, when both NO and CO molecules are adsorbed on Rh_4^+ cluster, there are two kinds of molecular complexes, a top-top $ONRh_4^+CO$ and a bridge-top $(ON)_bRh_4^+CO$, with the stabilization energies of 228.4 and 257.6 kJ mol^{-1} on their MERPs, respectively. It is obvious that the bridge-top $(ON)_bRh_4^+CO$ is more thermodynamically stable than the top-top $ONRh_4^+CO$. In $^3(ON)_bRh_4^+CO$, the spin densities of $-Rh_4$, –NO, and –CO moieties are 2.13, -0.11, and -0.02 *e*. It is indicated that the unpaired electrons mainly exist on $-Rh_4$ moiety. Moreover, the occupancies of each Rh-N and Rh-C bond orbitals are 1.93 *e*, indicating a complete single-bond in each Rh-N and in Rh-C. The bridge-top $(ON)_bRh_4^+CO$ may isomerizes into the top-top $ONRh_4^+CO$ with the energy barrier of 29.2 kJ mol^{-1} on their MERPs. From $ONRh_4^+CO$, there are two reaction pathways **RP-Pa** and **RP-Ps** to form a molecular complex $NRh_4^+CO_2$. On the **RP-Ps**, from $ONRh_4^+CO$, the C-O bond formation and N-O bond cleavage simultaneously take place via a five-member TS4-1, to produce a molecular complex $NRh_4^+CO_2$. Alternatively, on the **RP-Pa**, from $ONRh_4^+CO$, the N-O bond rupture to form a top-top NRh_4^+OCO via a four-member TS4-2. Next, from NRh_4^+OCO, a [1,2]-O shift occurs via a three-member TS4-3, to form a more top-bridge $NRh_4^+O_bCO$. Then, from $NRh_4^+O_bCO$, C-O bond formation occurs via a five-member TS4-4 to yield the molecular complex $NRh_4^+CO_2$. After that, $NRh_4^+CO_2$ releases the CO_2 molecule free, keeping NRh_4^+ behind. Last, from NRh_4^+, a [1,2]-N shift takes place via a three-member TS4-5, to produce a bridge $N_bRh_4^+$. This bridge $N_bRh_4^+$ deposits -305.4 kJ mol^{-1} in deep well on its MERP. In $^5N_bRh_4^+$, the spin densities of $-Rh_4$ and –N moieties are 4.15 and -0.15 *e*. It is indicated that the unpaired electrons mainly exist on $-Rh_4$ moiety. Moreover, the

Cite this: DOI: 10.1039/c0xx00000x

www.rsc.org/xxxxxx

Full Paper

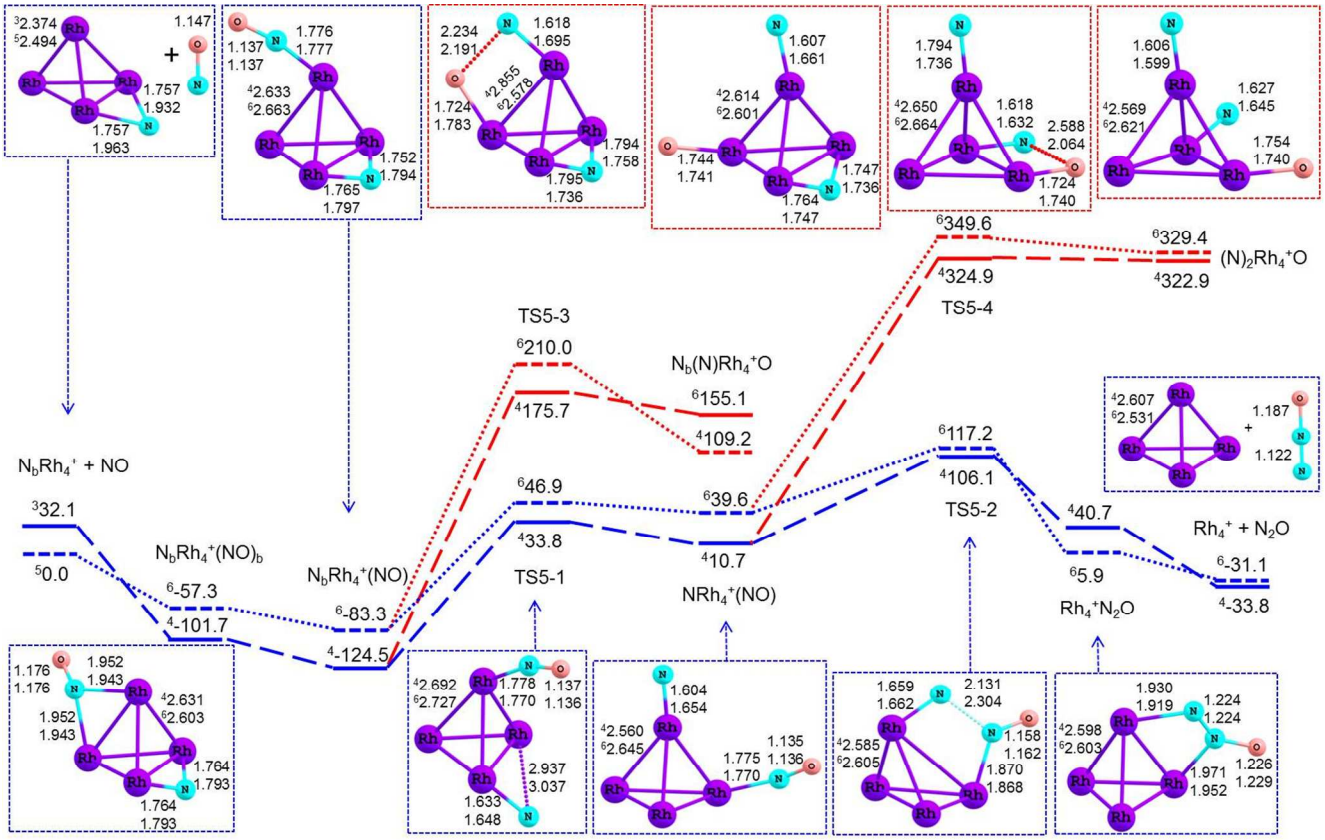

Fig. 5 The geometric structures of the reactants, intermediates, TSs, and products, and the schematic energy diagrams for the reaction (8) $N_bRh_4^+ + NO \rightarrow Rh_4^+ + N_2O$ calculated at the B3LYP/6-311+G(2d), SDD level. Bond lengths are reported in Å and bonds angles in degree. Relative energies (kJ mol^{-1}) for the corresponding species relative to $^5N_bRh_4^+ + NO$ are shown.

occupancies of two Rh-N bond orbitals are 6.48 *e*, indicating a triplet-bond in Rh-N-Rh. It is indicated that the bridge $N_bRh_4^+$ is thermodynamically preferred, which is in agreement with the experimental result of the existence of surface nitrogen.[48,49]

As indicated in Fig. 4, for the **RP-Ps**, the triplet-quintet spin crossing should take place once near TS4-1 via the MECP between $^3(ON)_bRh_4^+CO$ and $^5(ON)_bRh_4^+CO$. Thereby, the MERP should start at the sextet state and terminate on the quintet state, with the HEB of 248.9 kJ mol^{-1} at the C-O bond formation step of $^5ONRh_4^+CO \rightarrow {}^5$TS4-1 and the EHHP of 20.5 kJ mol^{-1} at ^{5}TS4-1. Alternatively, for **RP-Pa**, the triplet-quintet spin crossing should occur thrice near TS4-2 and TS4-4. Thereupon, the MERP should begin at the sextet state and end on the quintet state, with the HEB of 270.0 kJ mol^{-1} at the N-O bond cleavage step of $^5ONRh_4^+CO \rightarrow {}^5$TS4-2 and the EHHP of 41.6 kJ mol^{-1} at ^{5}TS4-2. Therefore, the **RP-Ps** is more kinetically favorable than the **RP-Pa**, because of its lower HEB and lower EHHP. In other words, the **RP-Ps** is dominant, compared with the **RP-Pa**. Furthermore, the MERP should begin at the quartet state and terminated on the quintet one.

3.2.2 $N_bRh_4^+ + NO \rightarrow Rh_4^+ + N_2O$

The geometric structures and the schematic energy diagrams for the reaction of (8) $N_bRh_4^+ + NO \rightarrow Rh_4^+ + N_2O$ are depicted in Fig. 5. As shown in Fig. 5, the reaction of (8) is calculated to be exergonic by 33.8 kJ mol^{-1} on its MERP. Thereby, this reaction is thermodynamically favorable.

As shown in Fig. 5, when the NO molecule is adsorbed on the bridge $N_bRh_4^+$ through N-end, there are two kinds of molecular complexes, a bridge-top $N_bRh_4^+(NO)$ and a bridge-bridge $N_bRh_4^+(NO)_b$, with the stabilization energy of 124.5 and 101.7 kJ mol^{-1} on its MERP. The bridge-top $N_bRh_4^+(NO)$ is more stable than the bridge-bridge $N_bRh_4^+(NO)_b$. In $^4N_bRh_4^+(NO)$, the spin densities of $-Rh_4$, –NO, and –N moieties are 3.04, -0.01, and -0.03 *e*. It is indicated that the unpaired electrons mainly exist on $-Rh_4$ moiety. Moreover, the occupancies of two Rh-N bond orbitals and Rh-NO bond orbitals are 5.82 and 1.82 *e*, respectively, indicating an about triplet-bond in Rh-N-Rh and an approximate single-bond in Rh-NO. From $N_bRh_4^+(NO)$, there are two reaction pathways. One is the [1,2]-N shift via a three-member TS5-1 to form a top-top $NRh_4^+(NO)$, and another is the N-O bond cleavage via a four-member TS5-3 to form a bridge-top-top $(N)_b(N)Rh_4^+O$. On their MERPs, ^{4}TS5-3 lies 141.9 kJ

Cite this: DOI: 10.1039/c0xx00000x

www.rsc.org/xxxxxx

Full Paper

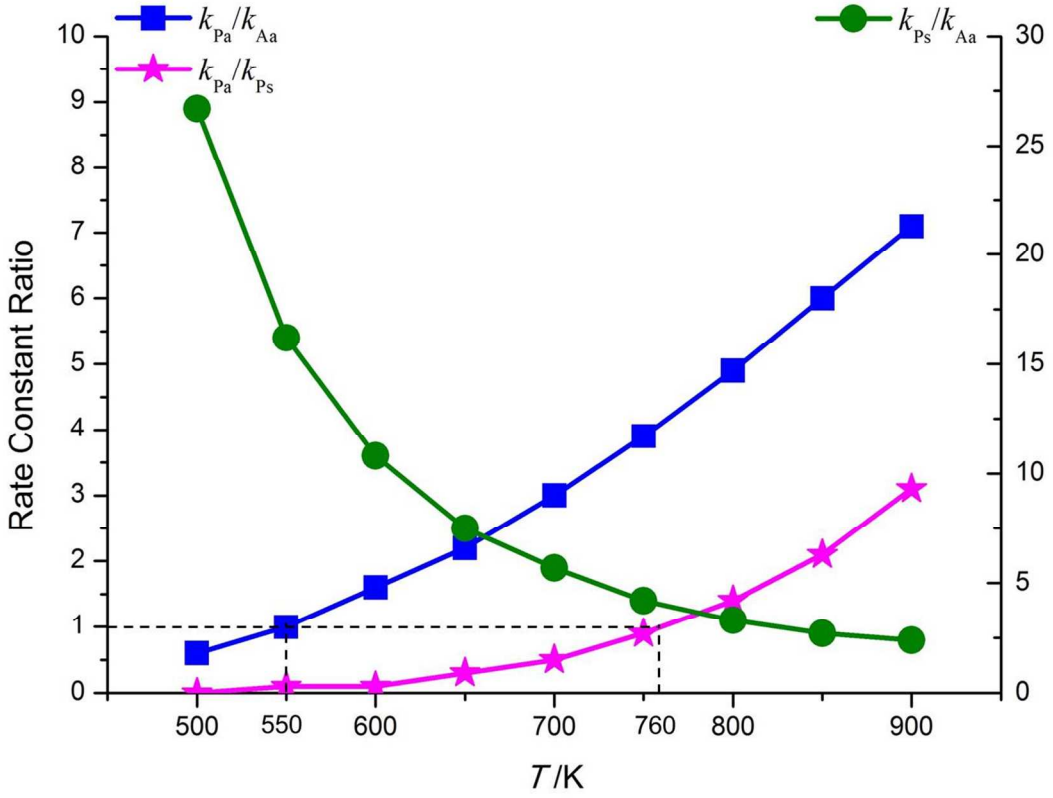

Fig. 6 The rate constant ratio as a function of temperature T in the $2NO + 2CO \rightarrow N_2 + 2CO_2$ reaction catalyzed on Rh_4^+ cluster calculated at the B3LYP/6-311+G(2d, 2p), SDD level. Blue, pink and green lines represent k_{Pa}/k_{Aa} k_{Pa}/k_{Ps}, and k_{Ps}/k_{Aa} respectively.

mol^{-1} above ^{4}TS5-1, and $^4(N)_b(N)Rh_4^+O$ deposits 98.5 kJ mol^{-1} above $^4NRh_4^+(NO)$. It is indicated that the reaction pathway of the [1,2]-N shift is more preferable both thermodynamically and kinetically than that of the N-O bond cleavage. After that, from $NRh_4^+(NO)$, there are also two reaction pathways. One is the N-N bond formation via a four-member TS5-2 through a [1,3]-N shift to form a molecular complex $Rh_4^+N_2O$, and another is the N-O bond scission via a four-member TS5-4 to a top-top-top $(N)_2Rh_4O$. On their MERPs, ^{4}TS5-4 locates 192.2 kJ mol^{-1} above ^{4}TS5-2, and $^4(N)_2Rh_4O$ lies 317.0 kJ mol^{-1} above $^6Rh_4^+N_2O$. It is indicated that the reaction pathway of N-N bond formation is more preferable both thermodynamically and kinetically than that of the N-O bond cleavage. That is to say, the reaction pathway of the N-N bond formation is predominant, compared with that of the N-O bond cleavage. Finally, $Rh_4^+N_2O$ set a N_2O molecule free without any energy requirement, keeping Rh_4^+ behind. For the reaction of (8) $N_bRh_4^+ + NO \rightarrow Rh_4^+ + N_2O$, the quartet-sextet spin crossing should take place thrice near TS5-1 and TS5-2. Then, the MERP should start at the quintet state and end on the quartet state, with the HEB of 158.3 kJ mol^{-1} at the N-shift reaction step of $^4N_bRh_4^+(NO) \rightarrow {}^4$TS5-1 and the EHHP of 106.1 kJ mol^{-1} at ^{4}TS5-2.

As mentioned earlier, for the gross reaction $NO + 2CO \rightarrow N_2 + 2CO_2$, there are two reaction pathways **RP-Pa** and **RP-Ps**. For the **RP-Pa** and **RP-Ps**, the TOF analysis showed that the TDIs are $^3(ON)_bRh_4^+CO$, and the TDTSs are ^{5}TS4-2 and ^{5}TS4-1, respectively. The TDI $^3(ON)_bRh_4^+CO$ are in charge of the NO and CO coadsorbed on Rh_4^+ cluster. The TDTSs (^{5}TS4-2 and ^{5}TS4-1) are responsible for the N-O bond cleavage, and the simultaneous C-O bond formation and N-O bond cleavage, respectively. Then, the rate constants of $^3(ON)_bRh_4^+CO \rightarrow {}^5$TS4-2 ($k_{Pa}$) and $^3(ON)_bRh_4^+CO \rightarrow {}^5$TS4-1 ($k_{Ps}$) are representative of the whole reaction constants of the **RP-Pa** and **RP-Ps**. Over the 300-900 K temperature range, the rate constants k_{Pa} and k_{Ps} can be fitted by the following expression (in s^{-1}):

$$k_{Pa} = 6.721\times10^{15}\exp(-318,376/RT) \quad \text{(v)}$$

$$k_{Ps} = 4.913\times10^{12}\exp(-272,724/RT) \quad \text{(vi)}$$

For convenience of comparison, the rate constant ratios of k_{Ps}/k_{Pa} and k_{Aa}/k_{Pa}, and k_{Ps}/k_{Aa} as a function of temperature T are computed. The $k_{Ps}/k_{Pa} \sim T$ and $k_{Aa}/k_{Pa} \sim T$ plots are depicted in Fig. 6. As shown in Fig. 6, the rate constant ratio k_{Ps}/k_{Pa} is greater than 1.0 at low temperature (300-760 K), whereas the rate constant ratio k_{Ps}/k_{Pa} is lower than 1.0 at high temperature (760-900 K). It

Cite this: DOI: 10.1039/c0xx00000x

www.rsc.org/xxxxxx

Full Paper

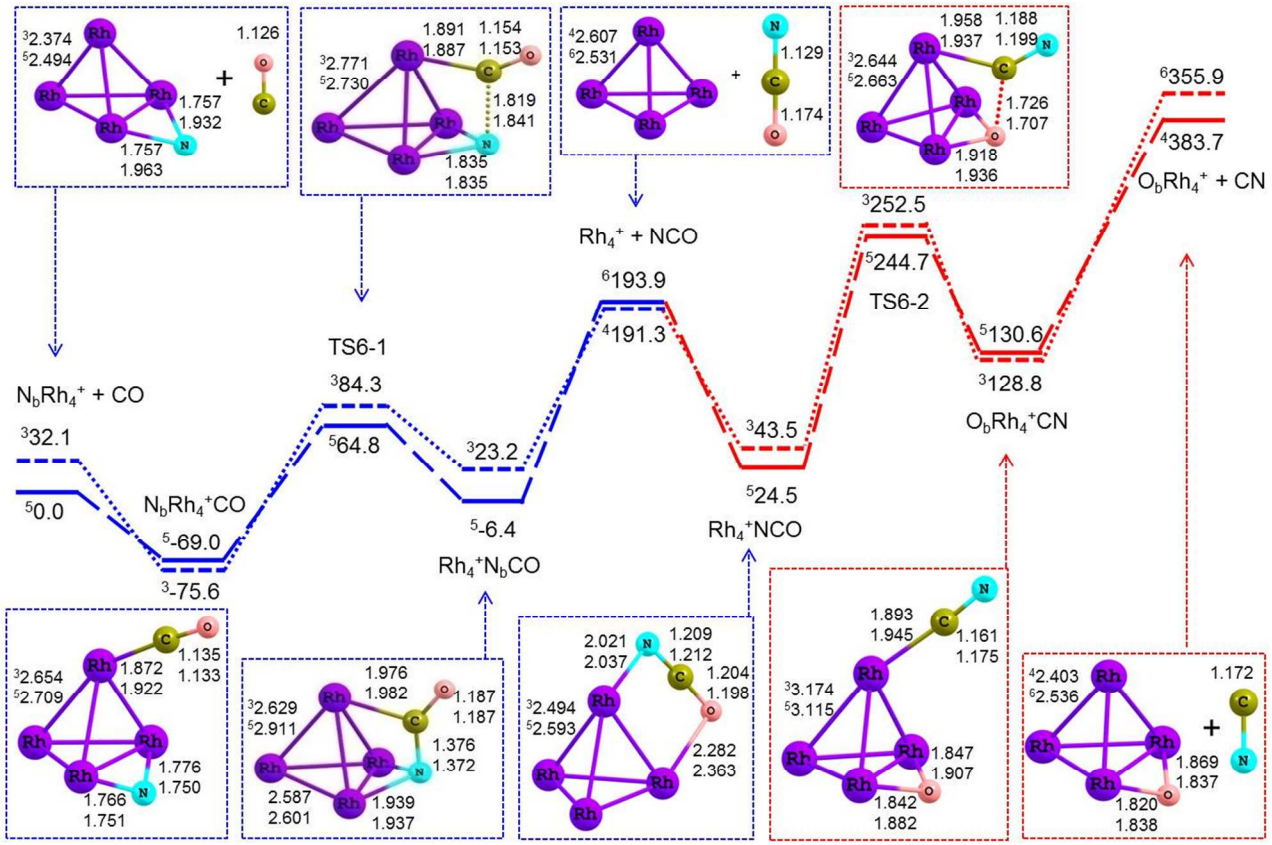

Fig. 7 The geometric structures of the reactants, intermediates, TSs, and products, and the schematic energy diagrams for the two reactions (9) and (10), that is, $N_bRh_4^+ + CO \rightarrow Rh_4^+ + NCO$ and $Rh_4^+ + NCO \rightarrow O_bRh_4^+ + CN$ calculated at the B3LYP/6-311+G(2d), SDD level, respectively. Bond lengths are reported in Å and bonds angles in degree. Relative energies (kJ mol^{-1}) for the corresponding species relative to $^5N_bRh_4^+ + CO$ are shown.

is indicated that the **RP-Ps** is more kinetically favorable than that of **RP-Pa** at low temperature (300-760 K), while the **RP-Pa** is more kinetically favorable than that of **RP-Ps** at high temperature (760-900 K).

As shown in Fig. 6, the rate constant ratio k_{Aa}/k_{Pa} is greater than 1.0 at low temperature (300-550 K), whereas the rate constant ratio k_{Aa}/k_{Pa} is lower than 1.0 at high temperature (550-900 K). It is indicated that the **RP-Aa** is more kinetically favorable than that of **RP-Pa** at low temperature (300-550 K), while the **RP-Pa** is more kinetically favorable than that of **RP-Aa** at high temperature (550-900 K).

Over the 300-900 K temperature range, the rate constant k_{Ps} is one time to three magnitude orders greater than the rate constant k_{Aa}. That is to say, the **RP-Ps** is dominant, compared with the **RP-Aa**.

In view of the rate constants of k_{Ps}, k_{Pa}, k_{Aa} and k_{Ap}, the rate constant k_{Ps} is the largest at low temperature (300-760 K), and the rate constant k_{Pa} dominant is the largest at high temperature (760-900 K). In other words, the **RP-Ps** is predominant at low temperature (300-760 K), while the **RP-Pa** is governed at high temperature (760-900 K). It is indicated that the presence of CO promotes the N-O bond cleavage on Rh_4^+ cluster. That is to say, the presence of CO in some degree decreases the catalytic reduction temperature of NO on Rh_4^+ cluster. This embodies the reducibility of CO toward NO, which promotes the reduction of NO. This result on Rh_4^+ cluster differs from that on Rh atom, in which CO plays a dominating role in the RhO reduction to regenerate Rh atom.[18] This may stem from the cooperativity of the Rh-Rh in Rh_4^+ cluster, which makes CO readily reduce NO.

In addition, at low temperature (300-760 K), the formation of CO_2 should originate in half from the reaction between the adsorbed CO and NO, which is in accordance to the experimental result by Brandt et al.[14] On the other hand, at high temperature (760-900 K), the formation of CO_2 should stem solely from the surface reaction between the adsorbed CO and O atom, the latter being originating from the NO decomposition, which is in agreement with the experimental observation.[15,17,50]

Considering the reduction of NO by CO, on the Rh_4^+ cluster, the optimal reaction pathways for RP-Ps and RP-Pa involve the EHHPs of 20.5 and 41.6 kJ mol^{-1} at ^{5}TS4-1 and ^{5}TS4-2 with the N-O bond cleavage, respectively. Alternatively, on the Rh_7^+ cluster, the optimal reaction pathway includes the EHHP of 0.0 kJ

mol^{-1} at the entrance reactants, with the N-O bond cleavage as the rate-determining step.[13] It is obvious that the EHHP on the Rh_4^+ cluster is higher than that on the Rh_7^+ cluster. One can see that the catalytic reactivity of Rh_7^+ cluster is stronger than that of Rh_4^+ cluster. This result embodies that the cooperativity of multi-rhodium centres is more beneficial to the N-O bond cleavage.

3.3 Formation of the NCO and CN side products

This reaction is composed of the two reactions (9) and (10), that is, $N_bRh_4^+ + CO \rightarrow Rh_4^+ + NCO$ and $Rh_4^+ + NCO \rightarrow O_bRh_4^+ + CN$. The geometric structures and the schematic energy diagrams for the reactions (9) and (10) are depicted in Fig. 7. As indicated in Fig. 7, the reactions of (9) and (10) are calculated to be endergonic by 183.0 and 375.9 kJ mol^{-1} on their MERPs, respectively. Accordingly, these two reactions (9) and (10) are thermodynamically hampered. However, as mentioned earlier, the reactions (2) and (3), that is, $NO + 2CO \rightarrow NCO + 2CO_2$ and $NO + 3CO \rightarrow CN + 2CO_2$, are calculated to be -114.1 and -74.5 kJ mol^{-1}, respectively. It is indicated that the two gross reactions are thermodynamically favorable.

3.3.1 $N_bRh_4^+ + CO \rightarrow Rh_4^+ + NCO$

As depicted in Fig. 7, first, when one CO molecule is adsorbed on $N_bRh_4^+$ through C-end, the molecular complex $N_bRh_4^+CO$ is generated with the stabilization energy of 75.6 kJ mol^{-1} on its MERP. In $^3N_bRh_4^+CO$, the spin densities of $–Rh_4$, –CO, and –N moieties are 2.12, -0.02, and -0.10 *e*. It is indicated that the unpaired electrons mainly exist on $–Rh_4$ moiety. Moreover, the occupancies of two Rh-N orbitals and one Rh-C bond orbitals are 6.58 and 1.96 *e*, respectively indicating a triplet-bond in Rh-N-Rh and a complete single-bond in in Rh-C. Next, from $N_bRh_4^+CO$, the C-N bond formation takes place via a five-member TS6-1, resulting in a molecular complex $Rh_4^+N_bCO$. Last, $Rh_4^+N_bCO$ releases the NCO molecule free, leaving Rh_4^+ behind. As indicated in Fig. 7, the triplet-quintet spin crossing should take place twice near TS6-1. Thereby, the MERP should start at the quintet state and terminate on the quartet, with the HEB of 197.7 kJ mol^{-1} at the releasing NCO step of $^5Rh_4^+N_bCO \rightarrow {}^4Rh_4 + NCO$ and the EHHP of 191.3 kJ mol^{-1} at the exit ($^4Rh_4^+ + NCO$).

As shown in Fig. 7, $^3N_bRh_4^+CO$ deposits -381.0 kJ mol^{-1} in deep well. The TOF analysis showed that for the NCO species formation the TDIs are $^3(ON)_bRh_4^+CO$ and $^3N_bRh_4^+CO$ with the degree of TOF control with 0.42 and 0.58, respectively, and the TDTS is ^{5}TS4-1 for N-O bond cleavage and C-O bond formation.

3.3.2 $Rh_4^+ + NCO \rightarrow O_bRh_4^+ + CN$

As shown in Fig. 7, when one NCO molecule is adsorbed on Rh_4^+ cluster, a μ-1,3-O,N molecular complex Rh_4^+NCO is obtained, with the stabilization energy of 166.8 kJ mol^{-1} on its MERP. From Rh_4^+NCO, the C-O bond cleavage takes place via a four-member TS6-2, leading to $O_bRh_4^+CN$. After that, from $O_bRh_4^+CN$, the direct Rh-C bond cleavage decomposes into $O_bRh_4^+$ moiety and CN radical.

As indicated in Fig. 7, the triplet-quintet spin crossing should take place near TS6-2. Thereupon, the MERP should begin on the quartet state and terminate on the sextet one, with the HEB of 247.1 kJ mol^{-1} at the reaction step of $^3O_bRh_4^+CN \rightarrow {}^6O_bRh_4^+ + CN$ and the EHHP of 355.9 kJ mol^{-1} at the exit $^6O_bRh_4^+ + CN$.

The TOF analysis showed that for the formation of CN species the TDI is $^3N_bRh_4^+CO$ and the TDTS exists at the exit ($^6O_bRh_4^+ + CN$). It is indicated that the release of CN radical is the TOF determining reaction step. This may be explained by the fact that $^3O_bRh_4^+CN$ involves the large complexation energy of 247.1 kJ mol^{-1} relative to $^6O_bRh_4^+ + CN$. Such large complexation energy impedes the release of CN species from $^3O_bRh_4^+CN$, trapping the $^3O_bRh_4^+CN$ complex in deep well.

As shown in Figs. 5 and 7, a glance to the reaction pathways reveals that the $^4N_bRh_4^+(NO)$ and $^5N_bRh_4^+CO$ intermediates are thermodynamically preferred. For the catalytic reduction of NO by CO catalyzed on Rh_4^+ cluster, the reaction traps the extremely stable complexes $^4N_bRh_4^+(NO)$ and $^5N_bRh_4^+CO$ in deep well. Once $N_bRh_4^+$ is formed, it is necessary to compare the reactions of $N_bRh_4^+$ with NO and CO. The reactions of $N_bRh_4^+ + NO \rightarrow Rh_4^+ + N_2O$ and $N_bRh_4^+ + CO \rightarrow Rh_4^+N_bCO$ are calculated to be exergonic by 33.8 and 6.4 kJ mol^{-1} on their MERPs, respectively, while the reaction of $N_bRh_4^+ + CO \rightarrow O_bRh_4^+CN$ is calculated to be endergonic by 128.8 kJ mol^{-1}. It is indicated that the two reactions of $N_bRh_4^+ + NO \rightarrow Rh_4^+ + N_2O$ and $N_bRh_4^+ + CO \rightarrow Rh_4^+N_bCO$ are thermodynamically preferable, whereas the reaction of $N_bRh_4^+ + CO \rightarrow O_bRh_4^+CN$ is thermodynamically unfavorable. However, the reaction $N_bRh_4^+ + CO \rightarrow Rh_4^+N_bCO$ is kinetically more favorable than the reaction $N_bRh_4^+ + NO \rightarrow Rh_4^+ + N_2O$ and $N_bRh_4^+ + CO \rightarrow O_bRh_4^+CN$, in virtue of its lower HEB (133.8 *vs* 158.3 and 220.2 kJ mol^{-1}) and lower EHHP (-240.6 *vs* -199.3 and -60.7 kJ mol^{-1}). These results indicate that from $N_bRh_4^+ + CO$, the reaction pathway for the $O_bRh_4^+CN$ formation should be ruled out, compared with those for $Rh_4^+ + N_2O$ and $Rh_4^+N_bCO$ the formation. In other words, on Rh_4^+ cluster, the N_2O and NCO contained species are predicted to be experimentally observed from the reduction of NO by CO, which is in good agreement with the experimental results.[20,51]

4. Conclusions

The catalytic reduction mechanism of NO by CO on the Rh_4^+ cluster has been extensively studied. The following conclusions can be drawn from the present calculations.

At low temperature (300-760 K), the reaction $2NO + 2CO \rightarrow N_2 + 2CO_2$ through **RP-Ps** is predominant, in which the TDTS is related to the simultaneous C-O bond formation and N-O bond cleavage. The reaction pathway includes five steps, (1) the coadsorption of NO and CO, (2) the recombination of CO and NO molecules to form CO_2 molecule and N atom, (3) the reaction of N atom with the second adsorbed NO to form N_2O, (4) the decomposition of N_2O to N_2 molecule and O atom, and (5) the recombination of O atom and CO to again form CO_2. The formation of CO_2 should originate in half from the reaction between the adsorbed CO and NO. The presence of CO in some degree decreases the catalytic reduction temperature of NO on Rh_4^+ cluster.

At high temperature (760-900 K), the reaction $2NO + 2CO \rightarrow N_2 + 2CO_2$ through **RP-Pa** is dominant, in which the TDTS is concerned to the N-O bond cleavage. The reaction pathway involves six steps, (1) the coadsorption of NO and CO, (2) the decomposition of NO to N and O atoms, (3) the recombination of CO and O atom to form CO_2, (4) the reaction of N atom with another adsorbed NO to form N_2O, (5) the decomposition of N_2O to N_2 molecule and O atom, and (6) the recombination of CO and

O atom to form CO_2. The formation of CO_2 should stem solely from the surface reaction between the adsorbed CO and O atom, the latter being originating from the NO decomposition.

The bridge $N_bRh_4^+$ is thermodynamically preferred, which is in agreement with the experimental result of the existence of surface nitrogen. Once the bridge $N_bRh_4^+$ is formed, the N_2O and NCO contained species are predicted to be experimentally observed from the reduction of NO by CO, which is in good agreement with the experimental results.

Acknowledgment

The authors are grateful for financial support by the National Natural Science Foundation of China (*No:* 21343001) and the Applied Foundation Research of Sichuan Province (*No*: 2011JY0024 and *No*: 2014JY0218).

Notes and references

[a] *College of Chemical Engineering, Sichuan University, Chengdu, Sichuan, 610065, P.R. China. Fax: 86 028 85415608; Tel: 86 028 85415608; E-mail: huaqingyang@scu.edu.cn*
[b] *Key Laboratory of Green Chemistry and Technology, Ministry of Education, College of Chemistry, Sichuan University, Chengdu, Sichuan, 610064, P.R. China.*

† Electronic Supplementary Information (ESI) available: [Thermal correction to Gibbs free energy (G_0, hartree), sum of electronic and thermal free energies (G_c, hartree), and relative energies (G_r, kJ mol^{-1}) various species with respect to the ground reactants calculated at the B3LYP/6-311+G(2d), SDD level in the gas phase under atmospheric pressure and room temperature (300 K and 1 atm). The standard orientations of various species calculated at the B3LYP/6-311+G(2d), SDD level in the catalytic reduction of NO by CO on the Rh_4^+ cluster.]. See DOI: 10.1039/b000000x/

1 S. L. Romo-Ávila and R. A. Guirado-López, *J. Phys. Chem. A*, 2012, **116**, 1059-1068.
2 O. R. Inderwildi, S. J. Jenkins and D. A. King, *J. Am. Chem. Soc.*, 2008, **130**, 2213-2220.
3 D. Chatterjee, O. Deutschmann and J. Warnatz, *Faraday Discuss.*, 2001, **119**, 371-384.
4 G. L. Gutsev, M. D. Mochena, E. Johnson and C. W. Bauschlicher, Jr., *J. Chem. Phys.*, 2006, **125**, 194312(1-11).
5 B. Hammer, *J. Catal.*, 2001, **199**, 171-176.
6 M. Shelef and G. W. Graham, *Catal. Rev.: Sci. Eng.*, 1994, **36**, 433-457.
7 M. L. Anderson, M. S. Ford, P. J. Derrick, T. Drewello, D. P. Woodruff and S. R. Mackenzie, *J. Phys. Chem. A*, 2006, **110**, 10992-11000.
8 M. S. Ford, M. L. Anderson, M. P. Barrow, D. P. Woodruff, T. Drewello, P. J. Derrick and S. R. Mackenzie, *Phys. Chem. Chem. Phys.*, 2005, **7**, 975-980.
9 P. Ghosh, R. Pushpa, S. de Gironcoli and S. Narasimhan, *J. Chem. Phys.*, 2008, **128**, 194708(1-8).
10 M. B. Torres, F. Aguilera-Granja, L. C. Balbás, and A. Vega, *J. Phys. Chem. A*, 2011, **115**, 8350-8360.
11 H. Xie, M. Ren, Q. Lei and W. Fang, *J. Phys. Chem. A*, 2011, **115**, 14203-14208.
12 C. D. Zeinalipour-Yazdi and R. A. van Santen, *J. Phys. Chem. C*, 2012, **116**, 8721-8730.
13 H. Xie, M. Ren, Q. Lei, W. Fang and F. Ying, *J. Phys. Chem. C*, 2012, **116**, 7776-7781.
14 M. Brandt, H. Müller, G. Zagatta, N. Böwering and U. Heinzmann, *Surf. Sci.*, 1996, **352-354**, 290-294.
15 C. H. F. Peden, D. N. Belton and S. J. Schmieg, *J. Catal.*, 1995, **155**, 204-218.
16 H. Permana, K. Y. Simon Ng, C. H. F. Peden, S. J. Schmieg, D. K. Lambert and D. N. Belton, *J. Catal.*, 1996, **164**, 194-206.
17 D. N. Belton, C. L. DiMaggio, S. J. Schmieg and K. Y. Simon Ng, *J. Catal.*, 1995, **157**, 559-568.
18 Q. Q. Xu, H. Q. Yang, C. Gao and C. W. Hu, *Struct. Chem.*, 2013, **24**, 13-23.
19 D. Lorimer and A. T. Bell, *J. Catal.*, 1979, **59**, 223-238.
20 A. Srinivasan and C. Depcik, *Catal. Rev.*, 2010, **52**, 462-493.
21 X. Ding, Z. Li., J. Yang, J. G. Hou and Q. Zhu, *J. Chem. Phys.*, 2004, **121**, 2558-2262.
22 V. P. Zhdanov and B. Kasemo, *Surf. Sci. Rep.*, 1997, **29**, 31-90.
23 M. J. Frisch, G. W. Trucks, H. B. Schlegel, G. E. Scuseria, M. A. Robb, J. R. Cheeseman, G. Scalmani, V. Barone, B. Mennucci, G. A. Petersson, H. Nakatsuji, M. Caricato, X. Li, H. P. Hratchian, A. F. Izmaylov, J. Bloino, G. Zheng, J. L. Sonnenberg, M. Hada, M. Ehara, K. Toyota, R. Fukuda, J. Hasegawa, M. Ishida, T. Nakajima, Y. Honda, O. Kitao, H. Nakai, T. Vreven, J. A. Montgomery, Jr., J. E. Peralta, F. Ogliaro, M. Bearpark, J. J. Heyd, E. Brothers, K. N. Kudin, V. N. Staroverov, T. Keith, R. Kobayashi, J. Normand, K. Raghavachari, A. Rendell, J. C. Burant, S. S. Iyengar, J. Tomasi, M. Cossi, N. Rega, J. M. Millam, M. Klene, J. E. Knox, J. B.Cross, V. Bakken, C. Adamo, J. Jaramillo, R. Gomperts, R. E. Stratmann, O. Yazyev, A. J. Austin, R. Cammi, C. Pomelli, J. W. Ochterski, R. L. Martin, K. Morokuma, V. G. Zakrzewski, G. A. Voth, P. Salvador, J. J. Dannenberg, S. Dapprich, A. D. Daniels, O. Farkas, J. B. Foresman, J. V. Ortiz, J. Cioslowski and D. J. Fox, GAUSSIAN 09 (Revision C.01), Gaussian Inc., Wallingford, CT, 2010.
24 A. D. Becke, *Phys. Rev. A*, 1988, **38**, 3098-3100.
25 C. Lee, W. Yang and R. G. Parr, *Phys. Rev. B*, 1988, **37**, 785-789.
26 A. D. McLean and G. S. Chandler, *J. Chem. Phys.*, 1980, **72**, 5639-5648.
27 R. Krishnan, J. S. Binkley, R. Seeger and J. A. Pople, *J. Chem. Phys.*, 1980, **72**, 650-654.
28 G. I. Mann, H. Stoll and H. Preuss, *Mol. Phys.*, 1988, **65**, 1321-1328.
29 R. Seeger and J. A. Pople, *J. Chem. Phys.*, 1977, **66**, 3045-3050.
30 R. Bauernschmitt and R. Ahlrichs, *J. Chem. Phys.*, 1996, **104**, 9047-9052.
31 C. Gonzalez and H. B. Schlegel, *J. Chem. Phys.*, 1989, **90**, 2154-2161.
32 C. Gonzalez and H. B. Schlegel, *J. Phys. Chem*., 1990, **94**, 5523-5527.
33 A. E. Reed, R. B. Weinstock and F. Weinhold, *J. Chem. Phys.*, 1985, **83**, 735-746.
34 A. Reed, L. A. Curtiss and F. Weihhold, *Chem. Rev.*, 1988, **88**, 899-926.
35 H. Eyring, *J. Chem. Phys.*, 1935, **3**, 107-115.
36 E. Winger, *J. Chem. Phys.*, 1935, **5**, 720-725.
37 S. Kozuch and S. Shaik, *J. Am. Chem. Soc.*, 2006, **128**, 3355-3365.
38 S. Kozuch and S. Shaik, *J. Phys. Chem. A*, 2008, **112**, 6032-6041.
39 A. Uhe, S. Kozuch and S. Shaik, *J. Comput. Chem.*, 2011, **32**, 978-985.
40 C. Amatore and A. Jutand, *J. Org. Chem.*, 1999, **576**, 254-278.
41 H. Eying, *J. Chem. Phys.*, 1935, **3**, 107-115.
42 C. Gao, H. Q. Yang, J. Xu, S. Qin and C. W. Hu, *J. Comput. Chem.*, 2010, **31**, 938-953.
43 M. Y. Yang, H. Q. Yang, C. Gao, S. Qin and C. W. Hu, *Struct. Chem.*, 2011, **22**, 983-997.
44 S. Qin, H. Q. Yang, C. Gao, J. Xu and C. W. Hu, *Surf. Sci.*, 2012, **606**, 1899-1905.
45 S. M. Hamilton, W. S. Hopkins, D. J. Harding, T. R. Walsh, P. Gruene, M. Haertelt, A. Fielicke, G. Meijer and S. R. Mackenzie, *J. Am. Chem. Soc.*, 2010, **132**, 1448-1449.
46 S. M. Hamilton, W. S. Hopkins, D. J. Harding, T. R. Walsh, M. Haertelt, C. Kerpal, P. Gruene, G. Meijer, A. Fielicke and S. R. Mackenzie, *J. Phys. Chem. A*, 2011, **115**, 2489-2497.
47 F. Rondinelli, N. Russo and M. Toscano, *J. Chem. Theory. Comput.*, 2008, **4**, 1886-1890.
48 J. Cortés and E. Valencia, *J. Phys. Chem. B*, 2006, **110**, 7887-7897.
49 J. Cortés and E. Valencia, *Phys. Rev. E*, 2005, **71**, 046136(1-10).
50 H. Permana, K. Y. Simon Ng, C. H. F. Peden, S. J. Schmieg, D. K. Lambert and D. N. Belton, *J. Catal.*, 1996, **164** , 194-206.
51 X. Ding, Z. Li, J. Yang, J. G. Hou and Q. Zhu, *J. Chem. Phys.*, 2004, **121**, 2558-2562.